AGU PUBLICATIONS

Geophysical Research Letters

RESEARCH LETTER
10.1002/2015GL065207

Key Points:
- We observe rapid slip pulses (velocity > 100 mm/s, acceleration>20 km/s) in laboratory stick-slip
- Pulses are common in lab experiments but cannot be detected without high-frequency instrumentation
- Pulses are migrating sources of high-frequency seismic radiation

Supporting Information:
- Figure S1
- Figure S2
- Figure S3
- Figure S4
- Figure S5
- Figure S6
- Figure S7
- Figures S1–S7 and Tables S1 and S2

Correspondence to:
G. C. McLaskey,
gcm8ster@gmail.com

Citation:
McLaskey, G. C., B. D. Kilgore, and N. M. Beeler (2015), Slip-pulse rupture behavior on a 2 m granite fault, *Geophys. Res. Lett.*, *42*, doi:10.1002/2015GL065207.

Received 2 JUL 2015
Accepted 12 AUG 2015
Accepted article online 14 AUG 2015

Slip-pulse rupture behavior on a 2 m granite fault

Gregory C. McLaskey[1], Brian D. Kilgore[2], and Nicholas M. Beeler[2]

[1]Cornell University, Ithaca, NY, USA, [2]U.S. Geological Survey, Menlo Park, California, USA

Abstract We describe observations of dynamic rupture events that spontaneously arise on meter-scale laboratory earthquake experiments. While low-frequency slip of the granite sample occurs in a relatively uniform and crack-like manner, instruments capable of detecting high-frequency motions show that some parts of the fault slip abruptly (velocity $> 100\,\mathrm{mm\,s^{-1}}$, acceleration $> 20\,\mathrm{km\,s^{-2}}$) while the majority of the fault slips more slowly. Abruptly slipping regions propagate along the fault at nearly the shear wave speed. We propose that the dramatic reduction in frictional strength implied by this pulse-like rupture behavior has a common mechanism to the weakening reported in high-velocity friction experiments performed on rotary machines. The slip pulses can also be identified as migrating sources of high-frequency seismic waves. As observations from large earthquakes show similar propagating high-frequency sources, the pulses described here may have relevance to the mechanics of larger earthquakes.

1. Introduction

The abruptness of rupture propagation during an earthquake is often described by the risetime, which is the duration of fault slip at a particular location on the fault upon passage of the rupture front. An earthquake is pulse-like if the risetime is short compared to the overall rupture duration. In crack-like rupture behavior (at the other end of a spectrum of rupture behavior) fault sections behind the rupture front continue to move until the end of the event. Earthquake risetime affects mechanics of fault rupture and the generation of potentially damaging seismic waves because it influences the peak slip velocity and acceleration. Since risetime is difficult to resolve from the inversion of earthquake ground motions [*Konka et al.*, 2013], modeling studies are required to test the implications of an assumed fault friction constitutive law (e.g., slip weakening and velocity weakening). Early rupture models that employed simplistic friction behavior resulted in crack-like ruptures with risetime determined by total rupture extent [e.g., *Kostrov*, 1964; *Madariaga*, 1976; *Day,* 1982], but it was recognized that an additional mechanism beyond a smoothly propagating, crack-like rupture was needed to account for the enhanced high-frequency energy observed in the spectra of earthquake seismograms [*Haskel*, 1964; *Brune*, 1970]. Citing waveform modeling studies that indicated short risetimes, *Heaton* [1990] proposed a slip-pulse rupture mode and suggested velocity-weakening friction as the most likely physical mechanism. Alternatively, *Beroza and Mikumo* [1996] found that velocity-independent friction was sufficient to model waveforms and cited heterogeneity as a possible mechanism for the inferred short risetimes.

Laboratory studies of rupture mode were initially conducted on thin plastic samples (~100 mm in size), and the stress field was measured optically. *Lykotrafitis et al.* [2006] and *Lu et al.* [2010] reported pulse-like ruptures that were artificially initiated with impact loading or thermal shock. *Nielsen et al.* [2010] reported pulse-like and mixed mode rupture when loading rapidly at 0.4 MPa/s. Other studies with lower loading rates have reported crack-like rupture behavior [*Latour et al.*, 2013; *Svetlizky and Fineberg*, 2014]. Recent large-scale experiments on rock samples also explore rupture behavior [e.g., *Fukuyama et al.*, 2013].

In this work, we describe slip-pulse rupture behavior observed in meter-scale rock friction experiments. We slowly load the samples and allow dynamic fault rupture to occur spontaneously. The large sample permits instrumentation that allows us to study the mechanics of the slip pulses, the conditions under which they form, and their relationship to high-frequency seismic waves generated during fault slip. Similar to the accounts by *Nielsen et al.* [2010], we observe extremely complex ruptures with trains of multiple slip pulses rupturing and rerupturing the fault within the wake of an overall crack-like nucleation process. Different from classic *Heaton* [1990] pulses, our observations indicate that pulses account for only a small amount of the total slip during an event and that most of the slip accumulates in a crack-like rupture process. Despite this, slip pulses are a primary source of high-frequency seismic waves radiated during the rupture, which may be key to linking the laboratory observations to the physics of larger, natural earthquakes.

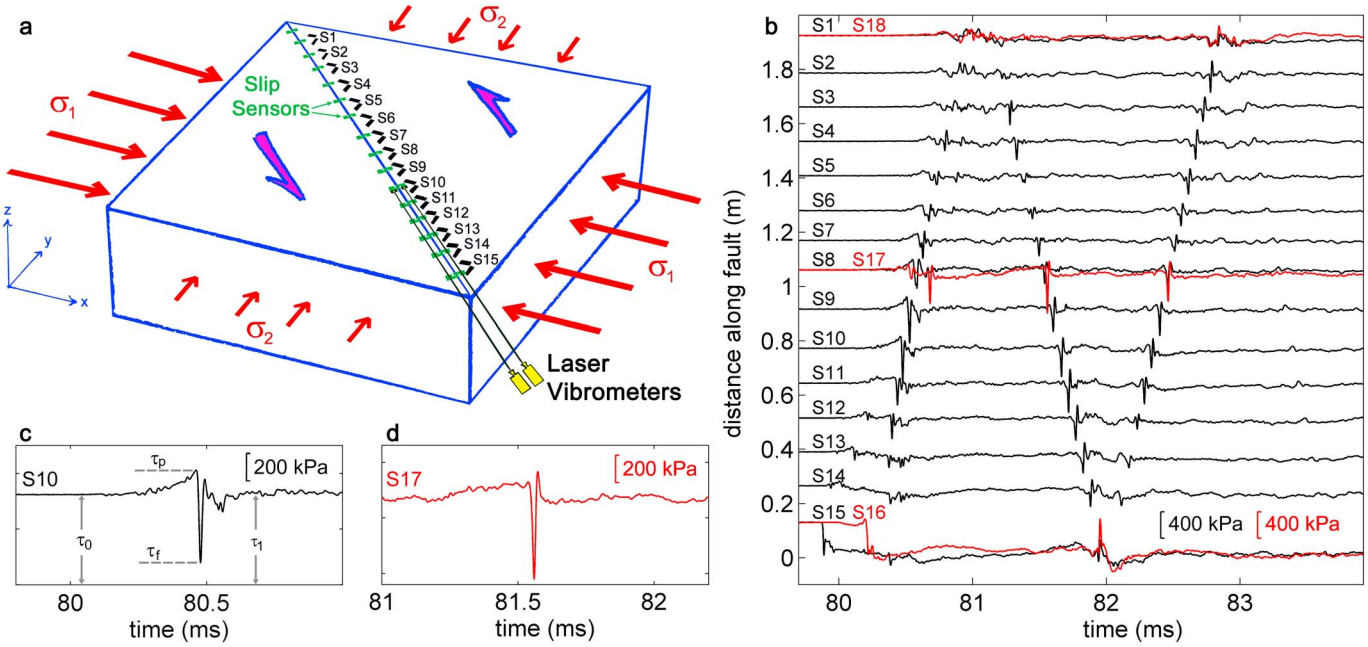

Figure 1. (a) A sketch of the large granite sample and saw cut fault (blue). Applied pressure (red arrows) is slowly increased to simulate tectonic stresses. Slow fault slip associated with a nucleation process culminates in rapid dynamic rupture of the entire fault, which we term a dynamic slip event (DSE). Local fault slip is measured at 16 locations along the top trace of the fault by capacitive slip sensors (green) that straddle the fault. (b) During a DSE, slip pulses can be identified by rapid fluctuations of shear stress measured by an array of strain gages (S1–S18) glued directly to the granite 13 mm from the fault trace. Traces from the 18 gages are offset by the gage location along the length of the fault. S16–S18 (red traces) are located on the bottom of the sample. The example DSE shown has a particularly simple pattern of slip pulses that propagate along the fault at $v_r = 2400$ m/s (±100 m/s) and reflect twice off the sample ends. The total duration of rapid slip during this DSE is 3.3 ms; it commences at about 80.15 ms and ceases at 83.45 ms. (c and d) Close-ups of stress fluctuations associated with slip pulses are characterized by a sudden drop in shear stress followed by a rapid recovery with essentially zero net change in shear stress.

2. Experimental Method

Experiments were performed on a large slab of granite 400 mm thick with a 2 m long simulated fault that is a diagonal saw cut, as shown schematically in Figure 1a [*Dietereich*, 1981; *Okubo and Dieterich*, 1984; *McLaskey and Kilgore*, 2013]. To roughly simulate slow tectonic loading, shear stress on the fault was slowly increased (0.001 to 0.01 MPa/s) while normal stress was held constant at 6 MPa. Under these conditions, slip begins slowly (<1 μm/s) in the center of the fault while the fault ends remain locked. The slipping region (or nucleation zone) expands while slip accelerates until it culminates with a dynamic slip event (DSE) that ruptures the entire 2 m fault [*McLaskey and Kilgore*, 2013]. The fault surface was initially prepared by lapping the two surfaces together with 30 grit abrasive, but the sample has been in use for more than 25 years and has sustained hundreds of slip events which may have smoothed the surfaces. While this sample is the "rough" fault, in the terminology of *Okubo and Dieterich* [1984], the sample is likely smoother and flatter than most natural faults, which causes the nucleation of dynamic slip to occur over smaller length scales and shorter time scales.

2.1. Local Fault Slip, Slip Rate, and Shear Stress

Fault slip is monitored with an array of capacitive slip sensors that straddle the top trace of the fault and measure local fault slip at 16 locations (see Figure 1a). These sensors are used to track the slow nucleation process, and they provide a low-resolution image of slip rate along the full length of the sample, but their frequency band (DC to 3 kHz) is too low to resolve the short-duration slip pulses.

The sample is also instrumented with a pair of laser vibrometers that measure local fault slip rate at frequencies up to 250 kHz at one location (see Figure 1a). The laser vibrometers record antisymmetric fault motion that can be integrated to provide a measure of fault slip that is consistent with the capacitive slip sensor measurements, as described in more detail the supporting information (Figures S1–S3). The high-frequency information obtained from the laser vibrometers reveals pulses where slip speeds exceed 100 mm/s for 20–40 μs bursts. As shown in Figure 2, these pulses are correlated with rapid fluctuations in shear stress observed from a line

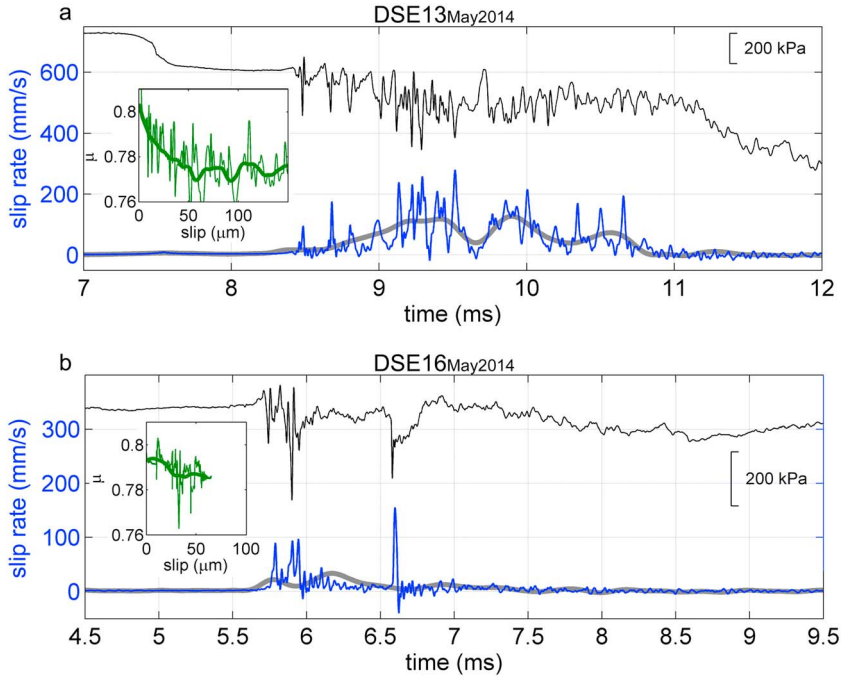

Figure 2. Correlation between collocated stress and slip rate measurements. Local shear stress (black) is obtained from a pair of strain gages located 13 mm from the fault trace (S10 from Figure 1). Sudden drops in local shear stress are correlated with brief pulses in local slip rate at the same location along the fault. The pulses are resolved by laser vibrometers with 250 kHz bandwidth (blue) but not capacitive slip sensors with 3 kHz bandwidth (thick grey). When local shear stress is plotted against cumulative fault slip (insets), the pulses resemble chatter riding atop standard slip weakening behavior. (Thick green lines show smoothed data.) (a) The rupture shown occurs at a larger overall stress level. The drop in shear stress at 7.5 ms is due to slow slip during quasistatic nucleation, whereas the first slip pulse reaches this location at about 8.4 ms. (b) The rupture shown occurs at a lower overall stress level. In this case, quasistatic nucleation processes occur before the time window shown.

of 15 strain gage pairs (S1–S15) (500 kHz bandwidth) that are glued to the rock surface 13 mm from the trace of the fault (Figure 1). As a slip pulse propagates past a strain gage location, it is identified by an abrupt drop in shear stress followed by a rapid recovery a few tens of microseconds later (Figures 1c and 1d). A complete list of sensor and data recording information is given in Table S1.

The extensive strain gage array allows us to track the rapid stress fluctuations that are indicative of slip pulses, so we can observe the initiation, propagation, and termination of slip pulses along the 2 m length of the fault. Once formed, slip pulses propagate along strike at an apparent velocity v_r that ranges from 2150 m/s to 2700 m/s (80% to 100% shear wave velocity). Most commonly, slip pulses originate at the sample ends once the slowly expanding, slowly slipping nucleation zone reaches this location. Consistent with previous studies [*Zheng and Rice*, 1998; *Lu et al.*, 2010], this scenario produces more pulse-like ruptures (see Figure 1, Figure 2b, Figure 3c, and Figure 3d), at lower levels of nondimensional shear stress (shear stress normalized by average normal stress, i.e., coefficient of friction). In such cases, pulses result from an interaction with the free boundary condition, which is less commonly encountered on natural faults. In other experiments, we observe slip pulses that originate within the interior of the sample (Figure 3a, between 8 and 9 ms), far from the somewhat artificial boundary conditions that most often generate the pulses. This occurs when slip nucleates at a higher level of nondimensional shear stress, and slip speeds in the nucleation region exceed ~1 mm/s before the nucleation zone expands all the way to the edge of the sample. These observations lead us to believe that slip pulses will develop spontaneously, irrespective of boundary conditions, once average slip speeds reach a critical level (~1 mm/s in the current experiments). Termination of slip pulses is characterized by a rapid attenuation of the stress field set up by the slip pulse, as described in the supporting information Figures S4–S6.

The laser-derived slip rate data (Figure 2) indicates that, in general, slip pulse duration $t_{pulse} = 20–40$ μs and total slip during each pulse $\delta_{pulse} \approx 2–4$ μm. (In contrast, a complete DSE has a slip duration of about

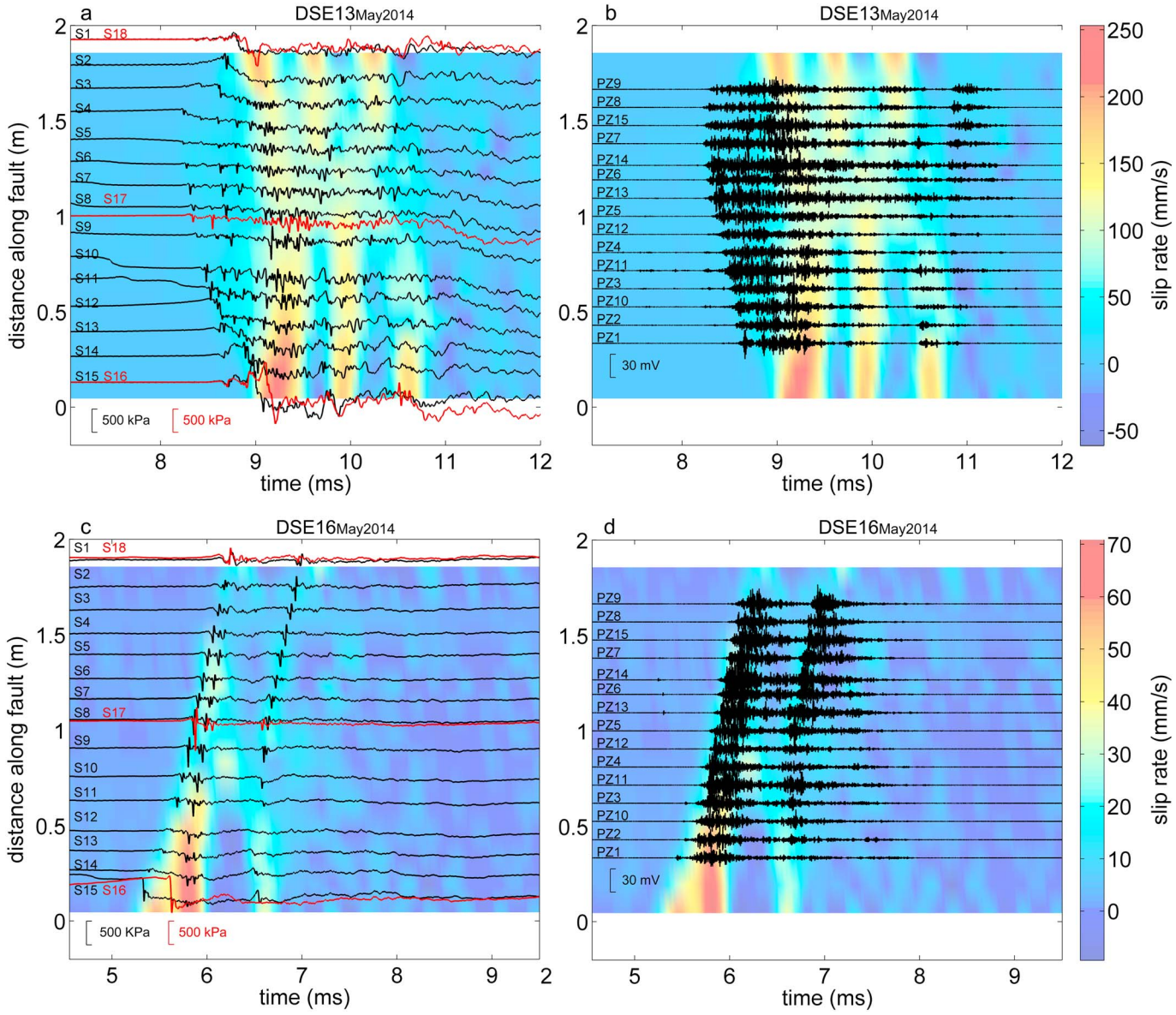

Figure 3. Maps of stress, sliprate, and high-frequency seismic radiation associated with two different dynamic ruptures on the 2 m fault. (a and c) Traces of local shear stress are offset by the gage location along the length of the fault and plotted on top of a color map of fault slip rate derived from data collected by an array of 16 capacitive slip sensors. The high-frequency slip pulses cannot be resolved with these sensors and therefore do not show up in this colormap. (b and d) Black traces are high-frequency vertical ground motions (100 to 500 kHz seventh-order Butterworth band pass) recorded from an array of piezoelectric sensors located 200 mm off the fault on both the top (PZ1, PZ3, PZ5, PZ7, PZ9, PZ10, PZ14, and 1PZ5) and bottom (PZ2, PZ4, PZ6, PZ8, PZ11, PZ12, and PZ13) of the 0.4 m thick granite sample. These traces are plotted on the same color maps as in Figures 3a and 3c for direct comparison of slip pulses and high-frequency seismic radiation. The time windows shown include only the dynamic culmination of slip events that also include a prolonged nucleation period described in detail in *McLaskey and Kilgore* [2013]. The dynamic slip shown here in the color maps complements the slow slip that accumulated during the nucleation process and is therefore nonuniform along strike. The DSE shown in Figures 3a and 3b started to nucleate near the center of the sample 100 s of milliseconds earlier, and the stress drops shown in Figure 3a at about 7.5 ms near S10 and S11 are due to slip associated with the expanding nucleation zone. Pulse-like rupture behavior initiated near the opposite edge of the expanding nucleation zone (near S4 or S5 at 8.2 ms) and propagated back through the nucleation zone. In contrast, the DSE shown in Figures 3c and 3d, nucleated more slowly and slow slip preferentially accumulated at one end of the sample (near S1). Pulse-like rupture behavior initiated when the expanding slow-slipping region reached the opposite end of the sample (near S15 at 5.7 ms).

3000 μs and a total slip of about 25–180 μm.) The width of the actively slipping zone within the slip pulse $x_{\text{pulse}} = t_{\text{pulse}} . v_r \approx 50$–$100$ mm and the average slip speed within pulses $\dot{\delta}_{\text{ave}} \approx 50$–$150$ mm/s (see supporting information Table S2). Additional strain gage pairs (S16–S18) mounted on the bottom of the sample indicate that slip pulses typically extend over the full 400 mm thickness of the fault, as shown in Figure 4, though 2-D effects are also observed, as described in the supporting information Figure S7.

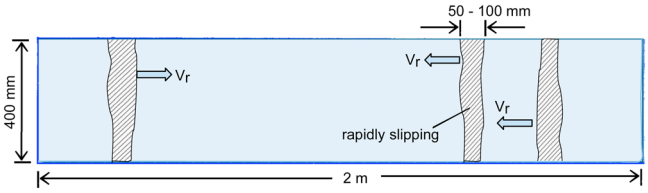

Figure 4. Cartoon of the fault cross section showing the approximate geometry of rapidly slipping regions.

Slip pulses of the type described here are extremely common in experiments of spontaneous rupture. For example, we have observed similar rapid fluctuations in strain gage data indicative of slip pulses in nearly every rupture experiment performed on the current apparatus. They are visible in Figure 7 of *McLaskey and Kilgore* [2013] and Figure 3b of *Beeler et al.* [2012]. Slip pulses are also the likely cause of the rapid fluctuations in shear stress shown in *Ohnaka and Kuwahara* [1990] (Figure 9 at 0.8 ms and Figure 10 at 0.7 ms), *Nielsen et al.* [2010] (Figure 4), *Latour et al.* [2013] (nearly horizontal white lines at about 28 ms in Figure 1), and *Fukuyama et al.* [2013] (Figures 5b and 10b). Without high-speed recording equipment, slip pulses would not be resolved, or they may be easily overlooked as noise.

In addition to the strain and slip sensors described above, the sample is instrumented with piezoelectric sensors that are the laboratory equivalent of seismometers. These sensors are located 200 mm from the fault trace on both the top and bottom of the sample, and they measure vertical ground motion in the 100 Hz to 1 MHz frequency band. We apply a high-pass filter to the recorded signals to remove the effects of lower frequency seismic waves that reflect off the boundaries of the sample and complicate the wavefield. The high-frequency signals left behind after filtering result from waves that attenuate rapidly with distance and therefore propagated directly from the nearby fault. They are used to map the approximate source location of the radiated (high-frequency) seismic waves with estimated spatial resolution of 200–400 mm. Using this technique, we find that seismic radiation of approximately constant power is spatiotemporally correlated with the slip pulses, as illustrated in Figure 3.

3. Discussion

Synthesis of the above observations paints the following picture: On first inspection, the fault appears to slip relatively uniformly during a DSE: the entire length of the fault slips about 100 microns for about 3 ms, with an average slip speed of about 20–60 mm/s. When we look in more detail with instruments that resolve higher frequency motion, we find that fault slip is far from uniform. As schematically depicted in Figure 4, small sections of the fault only 50–100 mm wide slip at rates of at least 100 mm/s while the rest of the fault slips at orders of magnitude lower rates (just a few mm/s). The rapidly slipping patches propagate along strike at about 2200–2600 m/s and often reflect off the free ends of the sample, but they only appear to propagate where they fault is already slipping at a lower rate. While these propagating slip pulses do not contribute to the majority of fault slip, they appear to produce the majority of the high-frequency seismic radiation.

What is the physical mechanism responsible for the slip pulses? The drop in shear stress associated with each pulse indicates that the shear stress supported locally by the fault is reduced dramatically when it slips rapidly but returns to $\mu = \sim 0.8$ levels just 50 μs later (Figure 2 insets) with essentially zero net change in shear stress. *Heaton* [1990] proposed velocity-weakening friction, but subsequent modeling studies found that the modest velocity-weakening behavior observed in low-velocity rock friction experiments [*Dieterich*, 1979; *Ruina*, 1983] was not enough to produce slip pulses [*Cochard and Madariaga*, 1994; *Perrin et al.*, 1995; *Beeler and Tullis*, 1996; *Zheng and Rice*, 1998]. The search for more intense weakening mechanisms led recent rock friction experiments to explore higher slip velocities where extremely low frictional strength was reported [*Tsutsumi and Shimamoto*, 1997; *Di Toro et al.*, 2004]. Though they have cited different mechanisms, including silica gel formation, powder lubrication, and flash melting of asperities [*Di Toro et al.,* 2004; *Reches and Lockner*, 2010; *Di Toro et al.,* 2011], these studies consistently place the onset of this intense weakening at slip rates of about 100 mm/s, which is consistent with the slip velocity threshold we observe for slip pulses. This suggests that similar mechanisms control both the slip pulses we observe and the rapid weakening observed in high-velocity friction experiments [*Liao et al.*, 2014; *Di Toro et al.*, 2011]. Indeed, we propose that the "chatter" that is universally observed in such experiments may be the result of pulse-like rupture behavior.

On the other hand, we observe slip pulses after only a few tens of microns of slip, while many rotary shear studies at similar stress levels showed that ~0.1 m of slip occurred before weakening took place [*Di Toro et al.*, 2011].

More recent work has shown that rapid slip acceleration, more representative of pulse-like loading, causes fault weakening to occur more rapidly and causes the fault to become more brittle [*Liao et al.*, 2014; *Chang et al.*, 2012; *Sone and Shimamoto*, 2009]. High-slip accelerations measured in our experiments during slip pulses ($>$20,000 m s^{-2}) suggest extreme brittleness (low fracture energy) and high seismic efficiency.

Additional mechanisms may be required to reduce the fracture energy enough for slip pulses to occur. For example, we have only seen slip pulses propagate where the fault was already actively slipping (at least ~ 1 μm/s), and we have not observed slip pulses that propagate outside of the "wake" of the more slowly expanding crack-like nucleation region (though the finite sample size limits scenarios when this would occur). This and the sudden termination of slip pulses (Figures S4–6) both suggest that the pulses cannot easily pass through stress barriers. The discrete, high-frequency foreshocks reported in an earlier study [*McLaskey and Kilgore*, 2013] may essentially be the seeds of slip pulses that were arrested by unfavorable conditions on the fault.

Similar to our observations, large natural earthquakes also generate moving sources of high-frequency seismic waves during dynamic rupture [*Spudich and Cranswick*, 1984; *Ishii et al.*, 2005; *Fletcher et al.*, 2006]. More recent studies illuminate extremely complex ruptures with intermittent and rapidly propagating sources of relatively high-frequency (~1 Hz) seismic waves within an overall slower rupture, as well as rerupture of certain fault sections [*Ishii*, 2011; *Meng et al.*, 2011, 2015]. Our results suggest that pulse-like rupture behavior may be the cause. However, many studies have suggested that high-frequency seismic radiation during large earthquakes is the result of frictional heterogeneities (i.e., asperities) or stress heterogeneities caused by residual stress concentrations left by past earthquakes. In our laboratory experiments, the smooth laboratory fault places tight constraints on fault complexity, and we measure negligible residual stresses over multiple stick-slip cycles [*McLaskey and Kilgore*, 2013]. Instead, we find that slip-pulse behavior and associated high-frequency radiation arises naturally from the dynamics of fault slip and does not result from some special material property or large barriers in either stress or strength. Though some mild form of heterogeneity is likely required to initiate them, slip pulses appear to be self-sustaining and are able to propagate through every part of the fault surface.

4. Conclusion

The laboratory observations presented here show that while the nucleation process and overall characteristics of slip instabilities are crack-like, rapid slip speeds ($<$1 mm/s) seem to promote the development of slip pulses. The slip pulses are initiated by a local release of elastic shear strain—either at the free ends of the sample or from some mild heterogeneity encountered at the edge of the expanding nucleation zone. Once formed, slip pulses are able to propagate rapidly (~2500 m/s) along the fault with negligible net stress change ($\tau_1 \approx \tau_0$, see Figure 1c). Slip pulses are only able to propagate where the fault is already slipping. Discrete foreshocks may effectively be slip pulses that were prematurely arrested because the fault had either not slipped enough or not slipped fast enough for fracture energy to be reduced to a level that would allow a slip pulse to propagate. While the abrupt slip pulses are not responsible for the majority of fault slip, they produce very rapid accelerations ($>$20 km/s^{-2}) and are a primary source of high-frequency seismic radiation. Additional work is required to understand how the mechanics of the laboratory observations might scale to larger ruptures at higher stress levels and on natural faults.

Acknowledgments

Data used in this paper were acquired during laboratory experiments at the U.S. Geological Survey in Menlo Park, California. Data can be made available by the authors upon request. This paper was improved by helpful discussions with Dave Lockner and reviews by Dave Lockner, Joe Fletcher, and Eric Dunham.

The Editor thanks Eric Durham for his assistance in evaluating this paper.

References

Beeler, N. M., and T. E. Tullis (1996), Self-healing slip pulses in dynamic rupture models due to velocity-dependent strength, *Bull. Seismol. Soc. Am.*, *86*(4), 1130–1148.

Beeler, N. M., B. Kilgore, A. McGarr, J. Fletcher, J. Evans, and S. R. Baker (2012), Observed source parameters for dynamic rupture with nonuniform initial stress and relatively high fracture energy, *J. Struct. Geol.*, *38*, 77–89.

Beroza, G. C., and T. Mikumo (1996), Short slip duration in dynamic rupture in the presence of heterogeneous fault properties, *J. Geophys. Res.*, *101*, 22,449–22,460, doi:10.1029/96JB02291.

Brune, J. N. (1970), Tectonic stress and the spectra of seismic shear waves from earthquakes, *J. Geophys. Res.*, *75*(26), 4997–5009, doi:10.1029/JB075i026p04997.

Chang, J. C., D. A. Lockner, and Z. Reches (2012), Rapid acceleration leads to rapid weakening in earthquake-like laboratory experiments, *Science*, *338*, 101–105.

Cochard, A., and R. Madariaga (1994), Dynamic faulting under rate dependent friction, *Pure Appl. Geophys.*, *142*(3–4), 419–445, doi:10.1007/BF00876049.

Day, S. M. (1982), Three-dimensional finite difference simulation of fault dynamics: Rectangular faults with fixed rupture velocity, *Bull. Seismol. Soc. Am.*, *72*(3), 705–727.

Di Toro, G., D. L. Goldsby, and T. E. Tullis (2004), Friction falls toward zero in quartz rock as slip velocity approaches seismic rates, *Nature*, *427*, 436–439, doi:10.1038/nature02249.
Di Toro, G., R. Han, T. Hirose, N. De Paola, S. Nielsen, K. Mizoguchi, F. Ferri, M. Cocco, and T. Shimamoto (2011), Fault lubrication during earthquakes, *Nature*, *471*, 494–498.
Dietereich, J. H. (1981), Potential for geophysical experiments in large scale tests, *Geophys. Res. Lett.*, *8*, 653–656, doi:10.1029/GL008i007p00653.
Dieterich, J. H. (1979), Modeling of rock friction: 1. Experimental results and constitutive equations, *J. Geophys. Res.*, *84*, 2161–2168, doi:10.1029/JB084iB05p02161.
Fletcher, J., P. Spudich, and L. Baker (2006), Rupture propagation of the 2004 Parkfield, California, Earthquake from observations at UPSAR, *Bull. Seismol. Soc. Am.*, *96*, S129–S142.
Fukuyama, E., K. Mizoguchi, F. Yamashita, H. Kawakata, and S. Takizawa (2013), How is a stick slip rupture initiatied?, Abstract T33C-2644 presented at 2013 Fall Meeting, AGU, San Francisco, Calif.
Haskel, N. A. (1964), Total energy and energy spectral density of elastic wave radiation from propagation faults, *Bull. Seismol. Soc. Am.*, *54*, 1811–1841.
Heaton, T. H. (1990), Evidence for and implications of self-healing pulses of slip in earthquake rupture, *Phys. Earth Planet. Inter.*, *64*(1), 1–20, doi:10.1016/0031-9201(90)90002-F.
Ishii, M. (2011), High-frequency rupture properties of the M_w 9.0 off the Pacific coast of Tohoku Earthquake, *Earth Planets Space*, *63*, 609–614.
Ishii, M., P. Sherer, H. Houston, and J. Vidale (2005), Extent, duration and speed of the 2004 Sumatra–Andaman earthquake imaged by the Hi-Net array, *Nature*, *435*, 933–936.
Konka, A. O., Y. Kaneko, N. Lapusta, and J.-P. Avouac (2013), Kinematic inversion of physically plausible earthquake source models obtained from dynamic rupture simulations, *Bull. Seismol. Soc. Am.*, *103*(5), 2621–2644.
Kostrov, B. V. (1964), Self similar problems of propagation of shear cracks, *J. Appl. Math. Mech.*, *28*(5), 1077–1087, doi:10.1016/0021-8928(64)90010–3.
Latour, S., A. Schubnel, S. Nielsen, R. Madariaga, and S. Vinciguerra (2013), Characterization of nucleation during laboratory earthquakes, *Geophys. Res. Lett.*, *40*, 5064–5069, doi:10.1002/grl.50974.
Liao, Z., J. Chang, and Z. Reches (2014), Fault strength evolution during high velocity friction experiments with slip-pulse and constant-velocity loading, *Earth Planet. Sci. Lett.*, *406*, 93–101.
Lu, X., A. J. Rosakis, and N. Lapusta (2010), Rupture modes in laboratory earthquakes: Effect of fault prestress and nucleation conditions, *J. Geophys. Res.*, *115*, B12302, doi:10.1029/2009JB006833.
Lykotrafitis, G., A. J. Rosakis, and G. Ravichandran (2006), Selfhealing pulse-like shear ruptures in the laboratory, *Science*, *313*(5794), 1765–1768, doi:10.1126/science.1128359.
Madariaga, R. (1976), Dynamics of an expanding circular fault, *Bull. Seismol. Soc. Am.*, *66*(3), 639–666.
McLaskey, G. C., and B. D. Kilgore (2013), Foreshocks during the nucleation of stick–slip instability, *J. Geophys. Res. Solid Earth*, *118*, 2982–2997, doi:10.1002/jgrb.50232.
Meng, L., A. Inbal, and J.-P. Ampuero (2011), A window into the complexity of the dynamic rupture of the 2011 M_w 9 Tohoku-Oki earthquake, *Geophys. Res. Lett.*, *38*, L00G07, doi:10.1029/2011GL048118
Meng, L., H. Huang, R. Burgmann, J.-P. Ampuero, and A. Strader (2015), Dual megathrust slip behaviors of the 2014 Iquique earthquake sequence, *Earth Planet. Sci. Lett.*, *411*, 177–187.
Nielsen, S., J. Taddeucci, and S. Vinciguerra (2010), Experimental observation of stick–slip instability fronts, *Geophys. J. Int.*, *180*(2), 697–702, doi:10.1111/j.1365-246X.2009.04444.x.
Ohnaka, M., and Y. Kuwahara (1990), Characteristic features of local breakdown near a crack-tip in the transition zone from nucleation to unstable rupture during stick–slip shear failure, *Tectonophysics*, *175*, 197–220.
Okubo, P. G., and J. H. Dieterich (1984), Effects of physical fault properties on frictional instabilities produced on simulated faults, *J. Geophys. Res.*, *89*, 5817–5827, doi:10.1029/JB089iB07p05817.
Perrin, G., J. R. Rice, and G. Zheng (1995), Self-healing slip pulse on a frictional surface, *J. Mech. Phys. Solids*, *43*(9), 1461–1495.
Reches, Z., and D. A. Lockner (2010), Fault weakening and earthquake instability by powder lubrication, *Nature*, *467*, 452–455.
Ruina, A. (1983), Slip instability and state variable friction laws, *J. Geophys. Res.*, *88*, 10,359–10,370, doi:10.1029/JB088iB12p10359.
Sone, H., and T. Shimamoto (2009), Frictional resistance of faults during accelerating and decelerating earthquake slip, *Nat. Geosci.*, *2*, 705–708.
Spudich, P., and E. Cranswick (1984), Direct observation of rupture propagation during the 1979 Imperial Valley earthquake using a short baseline accelerometer array, *Bull. Seismol. Soc. Am.*, *74*, 2083–2114.
Svetlizky, I., and J. Fineberg (2014), Classical shear cracks drive the onset of dry frictional motion, *Nature*, *509*, 205–208.
Tsutsumi, A., and T. Shimamoto (1997), High-velocity frictional properties of gabbro, *Geophys. Res. Lett.*, *24*(6), 699–702, doi:10.1029/97GL00503.
Zheng, G., and J. Rice (1998), Conditions under which velocity-weakening friction allows a self-healing versus a crack-like mode of rupture, *Bull. Seismol. Soc. Am.*, *88*(6), 1466–1483.